Journal of Photochemistry, 25 (1984) 419 - 438

$O_2(a\,^1\Delta_g)$-SENSITIZED CHEMILUMINESCENCE OF $a\,^1\Delta \rightarrow X\,^3\Sigma^-$ AND $b\,^1\Sigma^+ \rightarrow X\,^3\Sigma^-$ TRANSITIONS OF GROUP VI–GROUP VI AND GROUP V–GROUP VII DIATOMIC MOLECULES†

M. BIELEFELD, G. ELFERS, E. H. FINK, H. KRUSE, J. WILDT, R. WINTER and F. ZABEL

Fachbereich 9, Physikalische Chemie, Bergische Universität-GH Wuppertal, D-5600 Wuppertal 1 (F.R.G.)

(Received February 11, 1984)

Summary

The $b\,^1\Sigma^+(b0^+) \rightarrow X\,^3\Sigma^-(X_1 0^+, X_2 1)$ and $a\,^1\Delta(a2) \rightarrow X\,^3\Sigma^-(X_1 0^+, X_2 1)$ transitions of group VI–group VI and group V–group VII diatomic molecules in the near-IR spectral region were investigated by chemiluminescence measurements, excimer laser pulse photolysis and dye laser fluorescence. Spectroscopic identification of the $b \rightarrow X$ transitions of S_2, SeS and Se_2 and of the $a\,^1\Delta, v' = 0 \rightarrow X\,^3\Sigma^-, v'' = 0$ band of SO was achieved by comparing medium resolution Fourier transform IR spectra of the $O_2(a\,^1\Delta_g)$-sensitized chemiluminescence of these molecules with computer-simulated band shapes. Improved data for the electronic state energies of these molecules were obtained.

Time-resolved studies of the $b \rightarrow X$ emissions of SO, SeO, NI, PCl, PBr, SbF, SbCl and SbBr following excimer laser pulse photolysis of suitable parent compounds or pulsed dye laser excitation of the radicals in discharge flow systems are reported. From these studies preliminary data for the radiative lifetimes of the b states and quenching rate constants were deduced. The energy exchange and energy pooling processes operative in the $O_2(a\,^1\Delta_g)$-sensitized chemiluminescence systems and possible population inversions between the vibronic states are discussed.

1. Introduction

The dichalcogenides (group VI–group VI molecules) and the monohalides of the group V elements (group V–group VII molecules) represent two large groups of molecules exhibiting the same ... $(\pi^*)^2$ outer electronic configuration as O_2, the lightest species of the former group. Like O_2, the

†Paper presented at the COSMO 84 Conference on Singlet Molecular Oxygen, Clearwater Beach, FL, U.S.A., January 4 - 7, 1984.

0047-2670/84/$3.00

molecules have an $X^3\Sigma^-$ electronic ground state and low-lying $a^1\Delta$ and $b^1\Sigma^+$ excited states. The singlet states are metastable since the spin and orbital angular momentum selection rules forbid electric dipole transitions between the three states. For the heavier molecules increasing spin–orbit interaction leads to Hund's case c coupling. The $X^3\Sigma^-$ ground state is split into an $X_1 0^+$ and two converging $X_2 1^\pm$ substates. In the case c notation the excited states are designated a2 and $b0^+$ respectively. The selection rule $\Delta\Omega = 0, \pm 1$ now allows electric dipole transitions between the states which, however, remain much weaker than normal allowed transitions.

Whereas the $a^1\Delta$(a2) states are known only for a few of the molecules [1 - 4], the emission spectra from the $b^1\Sigma^+(b0^+)$ state to the ground state have now been observed in the gas phase for all 26 molecules of the two groups (excluding polonium- and bismuth-containing species). Low resolution studies of $O_2(a^1\Delta_g)$-sensitized chemiluminescence in discharge flow systems have proved to be especially fruitful in searching for the weak emission spectra. Applying this experimental method, during the last few years, we have succeeded in finding the previously unknown $b \rightarrow X$ emissions of 11 species (S_2 [5], SeS [6], Se_2 [6, 7], TeO [8], TeS [8], TeSe [9], Te_2 [7], AsCl [10], AsI [11], SbBr [12], SbI [11]) as well as the $a,v' = 0 \rightarrow X,v'' = 0$ band of SO [2].

For two more molecules (PI [13] and AsBr [10]) the available literature data over the $b \rightarrow X$ systems could be supplemented. In these studies the identification of the observed bands or band sequences was mostly based on the energy separations in band progressions, band shapes and Franck–Condon factor arguments. To confirm these identifications and to improve the spectroscopic constants deduced from the low resolution spectra, we have measured medium and high resolution spectra of the near-IR emissions of some of these molecules with a Fourier transform IR spectrometer. In addition, we have begun with experiments to determine the radiative lifetimes of the b states and to investigate the electronic quenching and energy exchange processes in collisions of the b state molecules with atomic or molecular gases. This information can be obtained by monitoring the time decay of the $b \rightarrow X$ emissions excited by excimer laser pulse photolysis of suitable parent compounds in static systems or by pulsed dye laser absorption in static as well as in discharge flow systems. Both experimental methods have successfully been applied to a number of molecules. Laser-induced fluorescence (LIF) excitation spectra were also obtained for the $b \rightarrow X_1$ transition of NI, the only system which had not been positively identified in the chemiluminescence studies [11, 14].

In this paper we present medium resolution Fourier transform IR spectra of the $b \rightarrow X$ transitions of S_2, SeS and Se_2, and of the $a,v' = 0 \rightarrow X,v'' = 0$ band of SO. By comparison of the band shapes with computer-simulated band contours the identification of the spectra is confirmed, and improved data for the electronic excitation energies are obtained. In addition we report some preliminary results of lifetime and quenching measurements and discuss the energy transfer processes and some possible population

inversions between vibronic states in the $O_2(a^1\Delta_g)$-sensitized chemiluminescence systems.

2. Experimental details

The flow system used for the chemiluminescence measurements was made of Pyrex glass and consisted of a tube 120 cm long of 10 cm diameter with quartz windows at both ends, two inlet systems of tubes 1.5 cm in diameter and two outlets at the other end leading to the pumping system and to a Baratron capacitance manometer. It was pumped with a 250 $m^3\ h^{-1}$ roots pump in series with a 30 $m^3\ h^{-1}$ forepump resulting in flow velocities of about 5 m s^{-1} in the observation tube of 10 cm diameter. In one of the inlet systems ground state SO, S_2, SeS or Se_2 radicals were produced by passing mixtures of helium carrier gas with respectively $SOCl_2$, S_2Cl_2, $S_2Cl_2 + Se_2Cl_2$ or Se_2Cl_2 vapour at a pressure of a few millitorrs through a microwave discharge. Through the second inlet oxygen containing about 5% of metastable $O_2(a^1\Delta_g)$ molecules was added to the gas flow. The $O_2(a^1\Delta_g)$ was produced in a second microwave discharge; most of the $O(^3P)$ atoms were removed from this gas stream by passing the oxygen over heated mercury before its passage through the microwave discharge. The total pressures were in the range 1 - 3 Torr (1 Torr ≡ 133 Pa), a normal mixture consisting of approximately equal amounts of O_2 and helium, and the dichloride vapours at a pressure of a few millitorrs.

The radiation emitted from the tube was focused onto the entrance diaphragm of a Nicolet model 7199 Fourier transform IR spectrometer with a quartz lens 10 cm in diameter. A flat aluminium mirror placed behind the window at the opposite end of the tube increased the intensity by about a factor of 2. The Fourier transform IR spectrometer was equipped with a germanium photodiode detector (RCA model TM 71 or Applied Detector Corporation model 403 L). The germanium detectors exhibit a high responsivity of about 10^9 V W^{-1} (noise equivalent power, 10^{-15} W $Hz^{-1/2}$ or less). Their sensitivity range extends from 0.7 to 1.7 μm with a maximum near 1.6 μm. However, because of the long time constant of the integrated liquid-nitrogen-cooled preamplifier, the frequency response of the detectors is limited to 10 - 500 Hz. The slowest possible mirror scanning velocity of the Fourier transform IR spectrometer was 0.08 cm s^{-1}, resulting in a frequency of 800 Hz for the interferogram of a line at 1 μm. Therefore, at short wavelengths the sensitivity of the detectors was limited to about 1.1 μm by their frequency response. The spectra of the $b \rightarrow X$ transitions of S_2, SeS and Se_2 between 1.2 and 1.5 μm were measured with the RCA detector which had a somewhat higher dynamic range and frequency response than the ADC model which, however, exhibited a higher sensitivity above 1.6 μm. The ADC detector, therefore, was used to measure the $a,v' = 0 \rightarrow X,v'' = 0$ band of SO at 1.706 μm. Because of its restricted dynamic range, an interference band filter had to be placed in front of this detector to shield it from other

radiation. The maximum spectral resolution achieved with the Fourier transform IR spectrometer was 0.08 cm^{-1}. To increase the signal-to-noise ratio of low intensity emission spectra, up to 1000 interferograms were coadded and averaged in the computer which also allowed data handling such as computation of spectra with different spectral resolution, addition or subtraction of spectra etc.

The experimental set-up for measuring time-resolved emissions following the excimer laser photolysis of suitable parent compounds has been described in a recent publication [15]. LIF studies were performed in the wavelength range 600 - 850 nm with an excimer-laser-pumped dye laser (Lambda Physik EMG 200 E/FL 2002 E), and in the range 850 - 1100 nm with an Nd:YAG-laser-pumped dye laser (Quantel model TDL III) equipped with a Raman cell (H_2, first and second Stokes lines) to shift the laser output to longer wavelengths.

Laser pulses of 5 - 20 mJ energy, about 10 ns pulse width, about 0.2 cm^{-1} linewidth and up to 10 Hz repetition frequency were obtained with the latter system in the region from 850 to 1100 nm. With the excimer-laser-pumped dye laser, depending on the wavelength and dye used, pulse energies up to 70 mJ at a linewidth of 0.05 cm^{-1} were achieved.

In the first LIF measurements reported here the ground state radicals were mostly produced in discharge flow systems using the same parent compounds as in the chemiluminescence studies. SO was also produced in a static system by excimer laser photolysis of SO_2 or $SOCl_2$ and after a time delay of 10 - 50 ms excited to the $b^1\Sigma^+$ state with the Raman-shifted dye laser output.

All chemicals and gases used were commercial and research grade and were used without further purification.

3. Results

3.1. Chemiluminescence measurements

$O_2(^1\Delta_g)$-sensitized chemiluminescence spectra of SO, S_2, SeS and Se_2 were measured with the Fourier transform IR spectrometer at a spectral resolution of 2 cm^{-1}. The band contours were computer simulated using rotational energy formulae from Kovacs [16] ($a^1\Delta$), Watson [17] ($X^3\Sigma^-$) and Herzberg [18] ($b0^+$, X_10^+, $X_21^\pm$) and the Hönl–London factors given by Kovacs [16]. The spectroscopic constants used for the calculations are collected in Table 1.

Figure 1 shows the SO($a^1\Delta, v' = 0 \rightarrow X^3\Sigma^-, v'' = 0$) band at 1.706 μm. The band was measured through an interference band filter with maximum transmission at 5760 cm^{-1} and a halfwidth of 240 cm^{-1}. Also, the sensitivity of the germanium detector drops steeply below 6000 cm^{-1}. The experimental band shape is not corrected for the resulting sensitivity change of the detection system. The band consists of nine branches [16]. The computed band shape agrees fairly well with the experimental trace. As was proved by

TABLE 1

Spectroscopic constants used in the band contour computations

State	B_0 (cm^{-1})	$10^6 \times D_0$ (cm^{-1})	γ_0 (cm^{-1})	λ_0 (cm^{-1})	*Reference*
$SO(X^3\Sigma^-)$	0.7179	1.12	−0.00562	5.278	[19, 20]
$SO(a^1\Delta)$	0.7112	1.17			[21]
$S_2(X^3\Sigma_g^-)$	0.2946	0.19	−0.0065	11.84	[1]
$S_2(b^1\Sigma_g^+)$	0.2873	0.21			Estimated
$SeS(X_10^+)$	0.1788	—			[1]
$SeS(X_21)$	0.1805	—			[1]
$SeS(b0^+)$	0.1731	—			Estimated
$Se_2(X_21)$	0.0900	—			[1]
$Se_2(b0^+)$	0.0874	—			Estimated

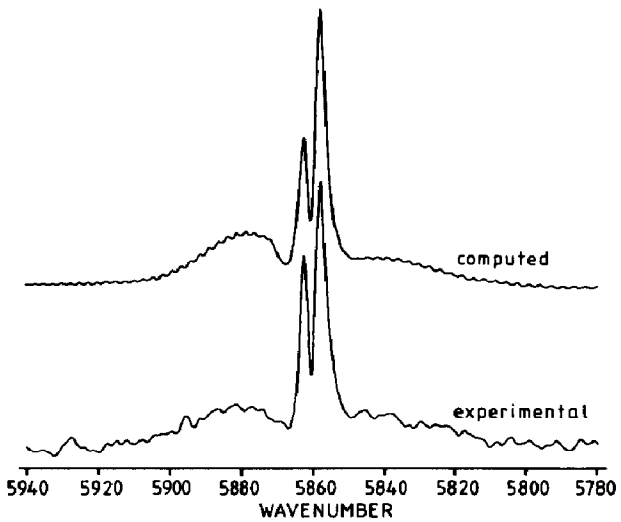

Fig. 1. Experimental and computer-simulated band contours of the $SO(a^1\Delta, v' = 0 \rightarrow X^3\Sigma^-, v'' = 0)$ band at 1.706 μm (T = 298 K; ν_{00} = 5861.9 cm^{-1}).

calibration measurements, the wavenumber scale of the Fourier transform IR spectrometer is correct to better than 0.02 cm^{-1} in the wavelength region studied in this work. By fitting the computed band maxima to the experimental band maxima the band origin could be determined to an accuracy of ±0.2 cm^{-1}.

Figures 2 - 4 show the spectra of the b → X transitions of S_2, SeS and Se_2. In Fig. 2, the $^1\Delta_g$ oxygen band at 7880 cm^{-1} which was superimposed on the $S_2(b, v' = 0 \rightarrow X, v'' = 0)$ band has been computer subtracted. For S_2, only the (0,0) and (0,1) bands are observed. The spectrum of SeS is very strong, and in addition to the (0,0) bands of both subtransitions $b0^+ \rightarrow X_10^+$ and $b0^+ \rightarrow X_21$ a number of bands from the $b0^+, v' = 1$ and $v' = 2$ levels are observed which originate from a near room temperature thermal population of these levels. Similarly, in the spectrum of Se_2, in addition to the (0,0)

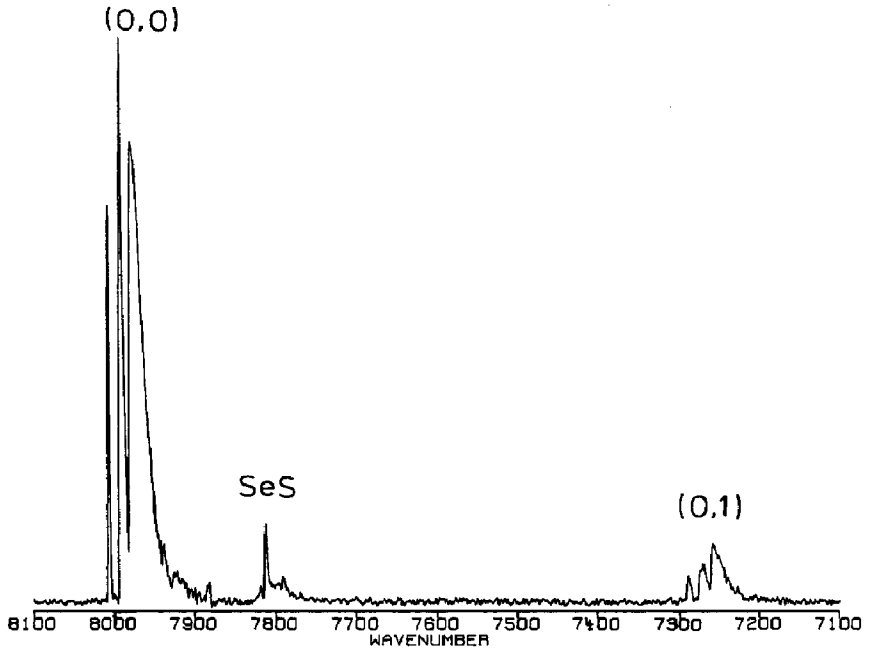

Fig. 2. Fourier transform IR spectrum of the $S_2(b^1\Sigma_g^+ \rightarrow X^3\Sigma_g^-)$ band system in the near-IR spectral region. The $O_2(a^1\Delta_g, v' = 0 \rightarrow X^3\Sigma_g^-, v'' = 0)$ band at 7880 cm^{-1} has been subtracted from the spectrum with the computer.

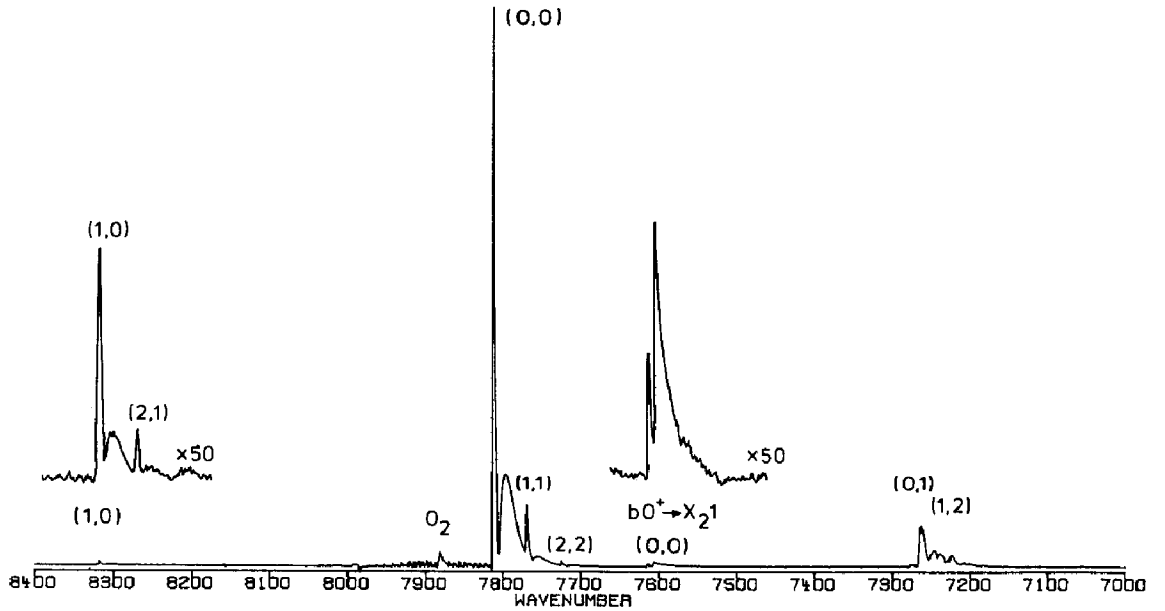

Fig. 3. Fourier transform IR spectrum of the $b0^+ \rightarrow X_1 0^+$ and $b0^+ \rightarrow X_2 1$ bands of SeS in the near-IR spectral region.

and (0,1) bands, the (1,1) and (2,2) bands are observed with intensities corresponding again to a near room temperature thermal population of the $v' = 0$, $v' = 1$ and $v' = 2$ levels. Figures 5 - 8 show the comparison of

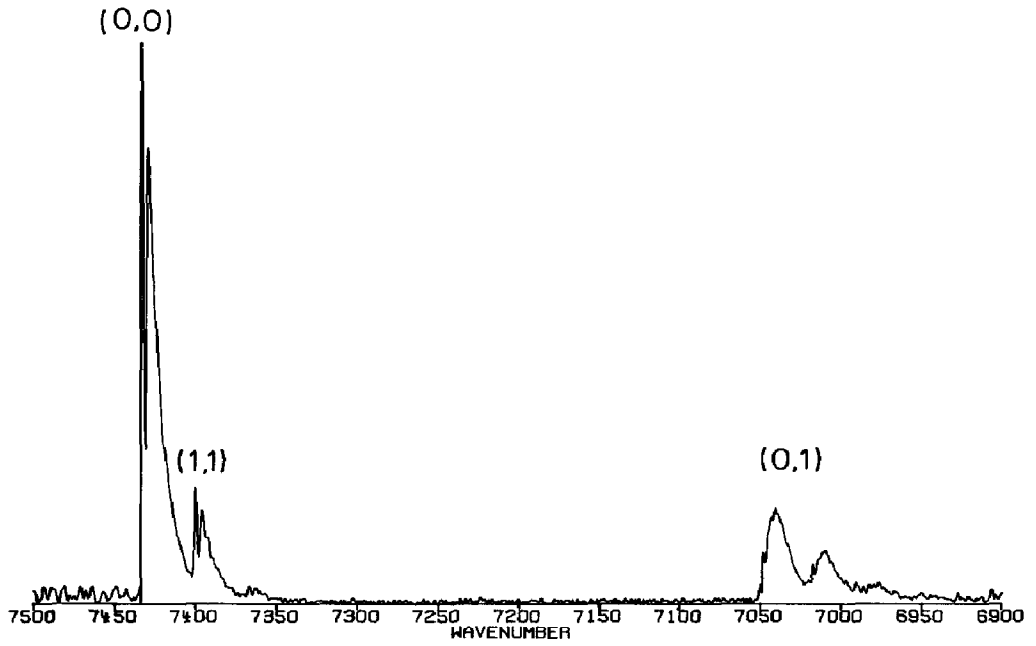

Fig. 4. Fourier transform IR spectrum of the $Se_2(b0^+ \rightarrow X_21)$ band system in the near-IR spectral region.

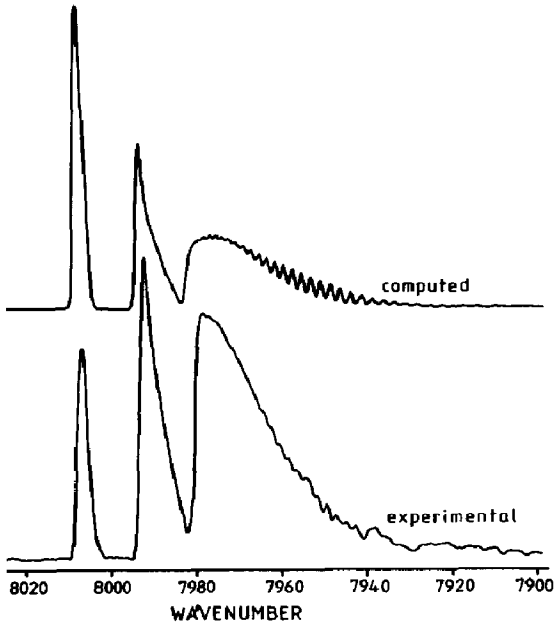

Fig. 5. Experimental and computer-simulated band contours of the (0,0) band of the $S_2(b \rightarrow X)$ system (T = 298 K; ν_{00} = 7981.5 cm^{-1}).

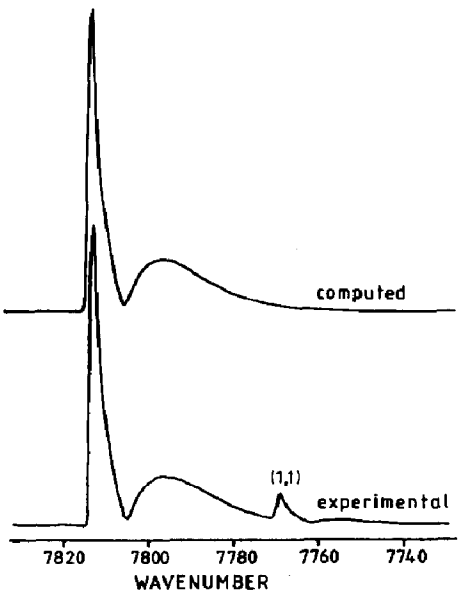

Fig. 6. Experimental and computer-simulated band contours of the (0,0) band of the $SeS(b \rightarrow X_1)$ system (T = 298 K; ν_{00} = 7805.4 cm^{-1}).

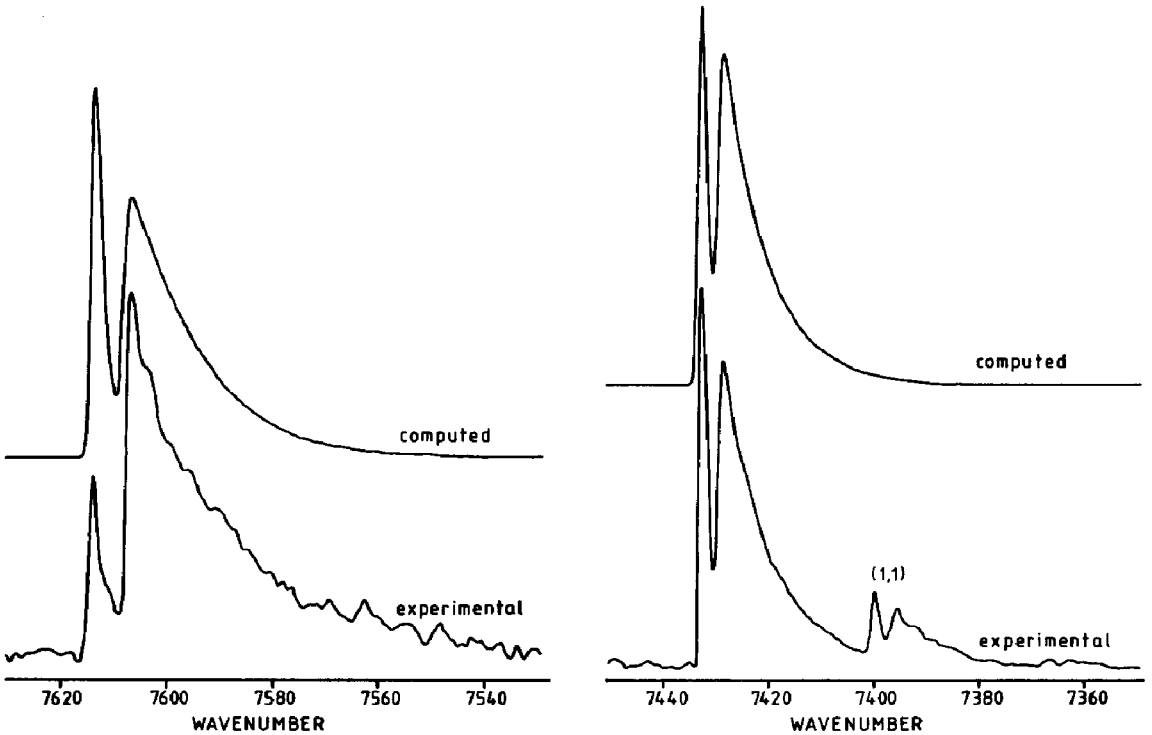

Fig. 7. Experimental and computer-simulated band contours of the (0,0) band of the SeS($b \rightarrow X_2$) system (T = 298 K; ν_{00} = 7608.0 cm^{-1}).

Fig. 8. Experimental and computer-simulated band contours of the (0,0) band of the Se_2($b \rightarrow X_2$) system (T = 298 K; ν_{00} = 7429.0 cm^{-1}).

the (0,0) bands with computer-simulated band shapes. Whereas for the SeS($b0^+ \rightarrow X_1 0^+$) and Se_2($b0^+ \rightarrow X_2 1$) transitions quite good agreement between the experimental and the computed band contours is found, for S_2($b\,^1\Sigma_g^+ \rightarrow X\,^3\Sigma_g^-$) and SeS($b0^+ \rightarrow X_2 1$) the computed bands show the same structure as the experimental bands but the relative intensities of the branches are substantially different. However, in all cases, by fitting the maxima of the experimental and computed bands, the band origins could be determined to an accuracy of ±1 cm^{-1}. The spectroscopic data obtained from the analysis of the spectra are collected in Table 2.

3.2. Excimer laser pulse photolysis and laser-induced fluorescence measurements

The experimental procedure, the data analysis and the problems associated with lifetime and quenching rate constant measurements of the metastable $b\,^1\Sigma^+$ states by excimer laser pulse photolysis have been described and discussed in a recent paper on SO($b\,^1\Sigma^+$) [15]. In continuation of this work we have studied the time decay of the $b \rightarrow X$ emissions of SeO, PCl, PBr and SbCl generated by ArF (193 nm) or KrF (248 nm) photolysis of $SeOCl_2$, PCl_3, PBr_3 and $SbCl_5$ respectively. The lifetimes and quenching rate

TABLE 2

Spectroscopic constants deduced from the Fourier transform IR spectra

Molecule	SO	S_2	SeS	Se_2
ν_{00}(a–X) (cm^{-1})	5861.9 ± 0.2			
ν_{00}(b–X) (cm^{-1})		7981.5 ± 1		
ν_{00}(b–X_1) (cm^{-1})			7805.4 ± 0.5	
ν_{00}(b–X_2) (cm^{-1})			7608.0 ± 1	7429.0 ± 1
$T_e(X_21)$ (cm^{-1})			197 ± 1	
T_e(a) (cm^{-1})	5879.2 ± 0.3			
T_e(b) (cm^{-1})			7827.7 ± 2	7955.0 ± 2
ω_e(b) (cm^{-1})			511 ± 2	355 ± 2

TABLE 3

Radiative lifetimes of the $a^1\Delta$ and $b^1\Sigma^+$ states of group VI–group VI and group V–group VII diatomic molecules

Molecule	$\tau(a^1\Delta)$ (s)	$\tau(b^1\Sigma^+)$ (ms)	*Method*[a]	*Reference*
O_2	3900	12000	Experimental: absorption	[22]
	5270	11650	Theoretical	[23]
SO	0.45	13.7	Theoretical	[23]
		5.7 ± 0.8	Experimental: ELP	[15]
		7 ± 2	Experimental: ELP–LIF	This work
S_2	350	2400	Theoretical	[23]
SeO		0.55 ± 0.05	Experimental: ELP	This work
		> 0.8	Experimental: DF–LIF	This work
NF	5.6		Experimental: DF	[24]
	3.1	16.5	Theoretical	[25]
		22.6 ± 1.7	Experimental: MD	[26]
NCl	0.53	1.9	Theoretical	[25]
		0.63 ± 0.06	Experimental: ELP	[27]
		0.25	Experimental: MD	[28]
NI		> 0.01	Experimental: DF–LIF	This work
PF		6.2 ± 0.7	Experimental: MD	[28]
PCl		2.0 ± 0.3	Experimental: ELP	This work
PBr		0.23 ± 0.05	Experimental: ELP	This work
		> 0.24	Experimental: DF–LIF	This work
SbF		> 0.15	Experimental: DF–LIF	This work
SbCl		0.37 ± 0.05	Experimental: ELP	This work
		> 0.34	Experimental: DF–LIF	This work
SbBr		> 0.45	Experimental: DF–LIF	This work

[a]ELP, excimer laser photolysis; ELP–LIF, excimer laser photolysis–LIF; DF–LIF, discharge flow–LIF; DF, discharge flow; MD, modulated discharge.

constants given in Tables 3 and 4 are preliminary data which have to be confirmed by further measurements. In fact, initial studies of the time decay of the SeO(b → X) fluorescence excited by the Raman-shifted dye laser in a

TABLE 4

Quenching rate constants for the $b^1\Sigma^+$ states of O_2, SO, SeO and PCl

Quencher	*Quenching rate constants* (cm^3 $molecule^{-1}$ s^{-1}) *for the* $b^1\Sigma^+$ *states of the following molecules*			
	O_2	*SO*	*SeO*	*PCl*
He	1×10^{-17} [29]	$< 1 \times 10^{-16}$ [15]	$< 5 \times 10^{-16}$	$< 1 \times 10^{-16}$
Ar	1.5×10^{-17} [29]	$< 1 \times 10^{-16}$ [15]	$< 5 \times 10^{-16}$	$< 1 \times 10^{-16}$
H_2	$(8.2 \pm 1.0) \times 10^{-13}$ [30]	$(1.2 \pm 0.2) \times 10^{-11}$ [15]	$(1.9 \pm 0.3) \times 10^{-11}$	$(4.5 \pm 0.6) \times 10^{-13}$
D_2	$(1.4 \pm 0.2) \times 10^{-14}$ [30]	$(1.3 \pm 0.3) \times 10^{-13}$ [15]	$(4.4 \pm 0.6) \times 10^{-13}$	$(1.7 \pm 0.3) \times 10^{-13}$
N_2	$(2.1 \pm 0.6) \times 10^{-15}$ [30, 31]	$(9.1 \pm 1.5) \times 10^{-14}$ [15]	$(1.3 \pm 0.2) \times 10^{-15}$	$< 1 \times 10^{-16}$
CO	5.6×10^{-15} [32]	$(1.7 \pm 0.3) \times 10^{-14}$ [15]	$(1.3 \pm 0.2) \times 10^{-12}$	$(4.0 \pm 0.6) \times 10^{-16}$
O_2	$(4.0 \pm 0.4) \times 10^{-17}$ [31]		$(1.2 \pm 0.2) \times 10^{-13}$	
CO_2	$(4.2 \pm 0.3) \times 10^{-13}$ [32, 33]	$(4.7 \pm 0.8) \times 10^{-13}$ [15]	$(1.2 \pm 0.2) \times 10^{-13}$	$(2.0 \pm 0.3) \times 10^{-14}$
SO_2	$(6.6 \pm 0.8) \times 10^{-16}$ [32, 33]	$\leq 1.9 \times 10^{-14}$ [15]		
CH_4	$(9.6 \pm 0.9) \times 10^{-14}$ [30]	$(4.5 \pm 1.2) \times 10^{-12}$ [15]	$(1.9 \pm 0.3) \times 10^{-11}$	$(2.0 \pm 0.3) \times 10^{-12}$

flow system indicate that the lifetime of the SeO($b^1\Sigma^+$) state may be substantially longer than the value of 0.55 ms obtained by extrapolation from the excimer laser pulse photolysis measurements. Likewise, the lifetimes of the b states of NI, PBr, SbF, SbCl and SbBr deduced from first LIF studies of the $b \rightarrow X$ systems of these species are lower limits only, since no systematic measurements of pressure dependences and studies of diffusion effects and other error sources have been performed yet.

4. Discussion

4.1. Spectra and energy levels

The Fourier transform IR spectra and the comparison of the experimental and computer-simulated band contours confirm the identification of the band systems given in our earlier work [2, 5 - 7]. The new energy values in most cases fall within the error limits of the previously given data. The energy splitting of the $X_1 0^+$ and $X_2 1$ sublevels of SeS of 197 ± 1 cm^{-1} is lower and more accurate than the value of 205 ± 7.5 cm^{-1} deduced from the Ω doubling in the $X_2 1$ state [34]. The substantial differences in the experimental and computed band shapes of the (0,0) bands of the $b^1\Sigma_g \rightarrow X^3\Sigma_g^-$ system of S_2 and the $b0^+ \rightarrow X_2 1$ subtransition of SeS (Figs. 5 and 7) indicate that, for these molecules which fall between Hund's cases b and c, the Hönl–London factors given by Kovacs [16] do not adequately reproduce the rotational line intensities. This problem will be further discussed in work on the rotational analysis of the S_2 and SeS bands [35]. The hitherto known $X_2 1$, $a^1\Delta(a2)$ and $b^1\Sigma^+(b0^+)$ state energies of the group VI–group VI and group V–group VII diatomic molecules are collected in Table 5. The b state energies which are now known for all 26 species have mostly been derived from emission spectra of the $b \rightarrow X$ transitions. Except for NBr, NI, PI and AsI, the ground state splittings in the heavier molecules are also known. However, in spite of some recent progress [2 - 4] the a state energies are still unavailable for 16 of the molecules, and for S_2 only an approximate value deduced from a matrix study is known. Where both states are known, the ratio of the a to b state energies lies between 0.5 and 0.65. Therefore, estimated values for the unknown $a \leftarrow X_1$ energies have been included in Table 5 by multiplying the $b \leftarrow X_1$ energies by 0.55.

4.2. Excitation processes in the chemiluminescence systems

Figures 9 - 11 show energy level diagrams of the low-lying states of the group VI–group VI and group V–group VII molecules. As is seen from Fig. 9, in the group VI–group VI molecules near resonances occur between the $a^1\Delta_g, v = 0$ state of O_2 and the $b, v = 0$ state energies of S_2, SeS, Se_2 and TeS. Energy exchange between these near-resonant levels is spin allowed and, therefore, probably proceeds very efficiently. In fact, as in the well-known $O_2(a^1\Delta_g)$–I system, collisional equilibria between the levels are established in the $O_2(a^1\Delta_g)$-containing chemiluminescence systems. This is demonstrated

TABLE 5

Excitation energies ν_{00} of group VI–group VI and group V–group VII molecules

Molecule	$\omega_e(X)$ (cm^{-1})	ν_{00} (cm^{-1})		
		$X_2 1$	$a^1\Delta(a2)$	$b^1\Sigma^+(b0^+)$
O_2	1580 [1]	—	7882 [1]	13121 [1]
SO	1149 [1]	—	5862[a]	10469 [1]
S_2	726 [1]	—	4395 [36][b]	7981[a]
SeO	915 [1]	166 [1]	5732 [3]	9685 [1]
SeS	556 [1]	197[a]	(4300)[c]	7805[a]
Se_2	385 [1]	510 [1]	(4370)[c]	7939[a]
TeO	797 [1]	789 [8]	(5460)[c]	9930 [8]
TeS	471 [1]	829 [8]	(4650)[c]	8446 [8]
TeSe	316 [1]	1235 [9]	(4830)[c]	8785 [9]
Te_2	247 [1]	1975 [37]	(5280)[c]	9591 [37]
NF	1141 [1]	—	11435 [1]	18905 [1]
NCl	827 [1]	—	9280 [4]	15039 [1]
NBr	692 [1]		9281 [4]	14834 [1]
NI	600 [14]		≈8460 [38][b]	13670 [14]
PF	847 [1]	—	7096 [1]	13364 [1]
PCl	577 [1]	—	(6660)[c]	12102 [1]
PBr	428 [1]		(6490)[c]	11809 [1]
PI	372 [13]		(6130)[c]	11150 [13]
AsF	686 [1]	139 [1]	7058 [1]	13654 [1]
AsCl	424 [10]	140 [10]	(6920)[c]	12587 [10]
AsBr	316 [10]	193 [10]	(6770)[c]	12317 [1]
AsI	257 [11]		(6460)[c]	11742 [11]
SbF	613 [1]	796 [1]	6818 [1]	13654 [1]
SbCl	375 [1]	816 [1]	(7130)[c]	12959 [1]
SbBr	257 [12]	874 [12]	(7020)[c]	12762 [12]
SbI	206 [11]	965 [11]	(6780)[c]	12330 [11]

[a] This work.
[b] From a matrix study.
[c] $0.55\nu_{00}(b–X_1)$.

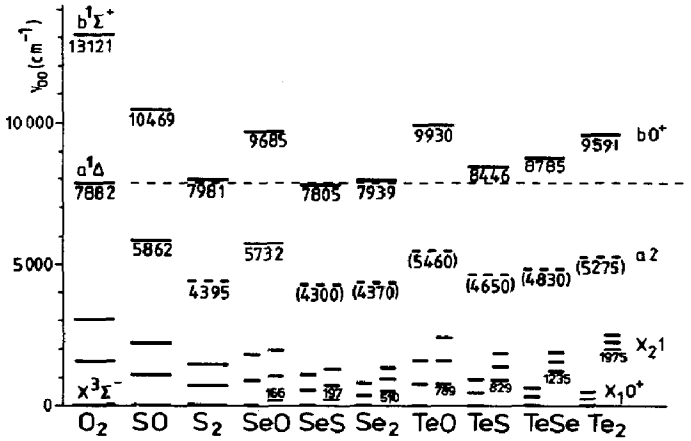

Fig. 9. Energy level diagram of the low-lying states of group VI–group VI molecules.

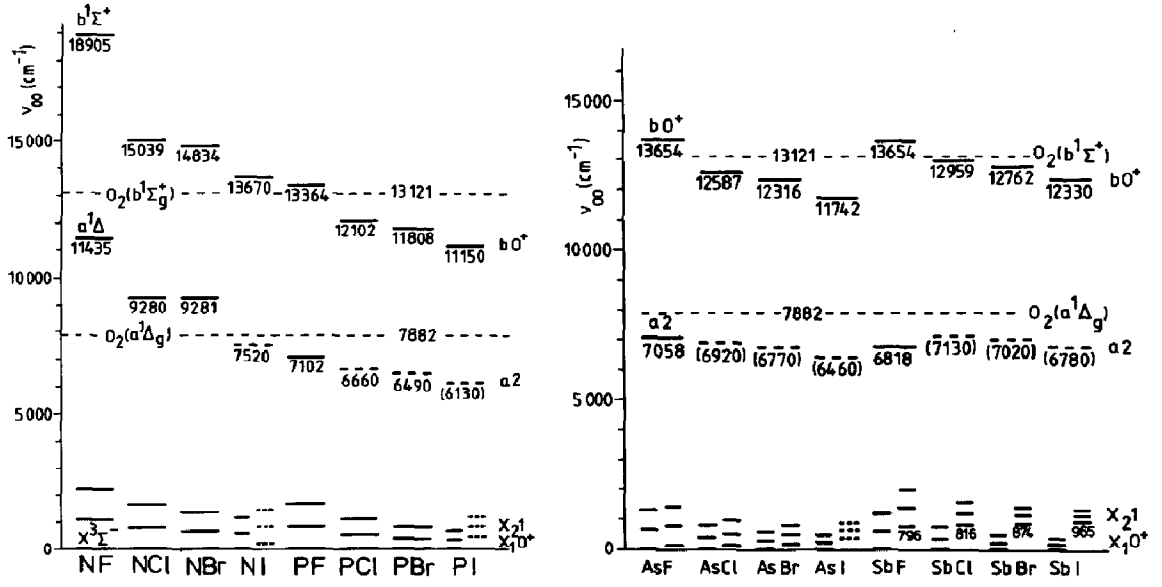

Fig. 10. Energy level diagram of the low-lying states of nitrogen and phosphorus monohalides.

Fig. 11. Energy level diagram of the low-lying states of arsenic and antimony monohalides.

by the finding that, on addition of foreign gases which do not affect $O_2(a^1\Delta_g)$ but quench the $b^1\Sigma^+$ states, the intensities of both the $b \rightarrow X$ emissions and the $O_2(a \rightarrow X)$ band decrease. This behaviour has been previously demonstrated for the $S_2(b \rightarrow X)$ bands [5]. It has also been observed in preliminary Stern–Volmer quenching measurements on the $b \rightarrow X$ emissions of SeS and Se_2 in the chemiluminescence systems. Whenever such an equilibrium is established, the concentration of $O_2(a^1\Delta_g)$ and the intensity of the band at 1.27 μm are strongly reduced [5 - 8]. Considering

$$O_2^*(a) + S_2(X) \underset{k_{-1}}{\overset{k_1}{\rightleftharpoons}} O_2(X) + S_2^{**}(b) \tag{1}$$

$$O_2^*(a) \xrightarrow{k_{O_2^*}^r} O_2(X) + h\nu \tag{2}$$

$$S_2^{**}(b) \xrightarrow{k_{S_2^{**}}^r} S_2(X) + h\nu \tag{3}$$

and using the equilibrium assumption

$$K = \frac{k_1}{k_{-1}} = \frac{[O_2][S_2^{**}]}{[O_2^*][S_2]} \tag{4}$$

the intensity ratio of the $S_2(b \rightarrow X)$ and $O_2(a \rightarrow X)$ emissions is given by

$$\frac{I_{S_2^{**}}}{I_{O_2^*}} = \frac{k_{S_2^{**}}{}^{r}[S_2^{**}]}{k_{O_2^*}{}^{r}[O_2^*]}$$

$$= K \frac{k_{S_2^{**}}{}^{r}}{k_{O_2^*}{}^{r}} \frac{[S_2]}{[O_2]} \tag{5}$$

Since the rotational and vibrational energies in the X, a and b states are very similar for both molecules, the statistical expression for the equilibrium constant reduces to

$$K \approx \exp\left(-\frac{\Delta E}{kT}\right) \tag{6}$$

For the O_2–S_2 system with $\Delta E \approx 100$ cm^{-1}, $K \approx 0.6$ and with the lifetime data of Table 3 it is estimated that

$$\frac{k_{S_2^{**}}{}^{r}}{k_{O_2^*}{}^{r}} = \frac{\tau_{O_2^*}}{\tau_{S_2^{**}}} = \frac{3900\ \text{s}}{2.4\ \text{s}} = 1625 \tag{7}$$

Thus

$$\frac{I_{S_2^{**}}}{I_{O_2^*}} \approx 1000 \frac{[S_2]}{[O_2]} \tag{8}$$

is obtained for the intensity ratio. Under typical experimental conditions, *e.g.* with O_2 at a pressure of about 1 Torr and S_2Cl_2 at a pressure of a few millitorrs, the observed intensity ratio is between 1 and 5, which would mean that the ground state S_2 concentration is in the millitorr range, *i.e.* of the same order of magnitude as the S_2Cl_2 parent gas pressure, which seems to be a reasonable result supporting in turn the theoretical value for the lifetime of the $S_2(b\,^1\Sigma^+)$ state. For the heteronuclear molecule SeS the lifetime of the b state is expected to be at least three orders of magnitude shorter than for S_2 (see Table 3). From the observed typical intensity ratios of about 100 it is estimated that the ground state SeS concentration is lower by a factor of 10 - 100 than the S_2 concentration in the O_2–S_2 system. This is in accord with the less efficient production of SeS from mixtures of S_2Cl_2 and Se_2Cl_2 and the observation that traces of SeS from the wall of the flow tube give quite strong SeS(b → X) emission.

For SO, SeO, TeO and Te_2 as well as for all group V–group VII molecules no direct excitation of the b states by $O_2(a\,^1\Delta_g)$ is possible. However, in nearly all cases the presence of $O_2(a\,^1\Delta_g)$ is a necessary condition for the observation of the b → X emission spectra, or the intensity of the emissions is increased if $O_2(a\,^1\Delta_g)$ is added to the system. For the $O_2(a\,^1\Delta_g)$–SO system it has been shown [2, 39] that energy transfer to $SO(a\,^1\Delta)$

$$O_2^*(a) + SO(X) \rightarrow O_2(X) + SO^*(a) \tag{9}$$

for which $k_9 = 3.5 \times 10^{-13}$ cm^3 molecule^{-1} s^{-1} [40], followed by energy pooling processes

$$SO^*(a) + O_2^*(a) \longrightarrow SO^{**}(b) + O_2(X) \quad (10a)$$

$$SO^*(a) + O_2^*(a) \longrightarrow SO(X) + O_2^{**}(b) \quad (10b)$$

$$SO^*(a) + SO^*(a) \longrightarrow SO^{**}(b) + SO(X) \quad (11)$$

is the most likely excitation pathway of $SO(b^1\Sigma^+)$. Similarly, a major role of energy pooling processes has been proved in the $I^*-O_2^*$, $O_2^*-NF^*$ and I^*-NF^* systems [41 - 43]. Therefore, it is highly probable that also for SeO, TeO and Te_2 and with most group V–group VII molecules corresponding energy transfer and energy pooling processes are operative. As is seen from Figs. 10 and 11, with some group V–group VII molecules close energy resonances between the b states and the $b^1\Sigma_g^+$ state of O_2 occur. However, direct exchange of the b state energies has not yet been observed.

Except for k_9 the rate constants of the energy transfer processes operative in the $O_2(a^1\Delta_g)$-sensitized chemiluminescence systems are not known. However, it can be assumed that the near-resonant processes between $O_2(a^1\Delta_g)$ and S_2, SeS, Se_2 and TeS are much faster and exhibit close to gas kinetic cross sections as for the energy transfer process from $O_2(a^1\Delta_g)$ to iodine atoms:

$$O_2^*(a) + I(^2P_{3/2}) \longrightarrow O_2(X) + I^*(^2P_{1/2}) \quad (12)$$

for which $k_{12} = 7.6 \times 10^{-11}$ cm^3 molecule^{-1} s^{-1} [44].

4.3. Radiative lifetimes

The radiative lifetimes of the $b^1\Sigma^+(b0^+)$ states deduced from the excimer laser pulse photolysis and the LIF studies fall in the range 0.1 - 10 ms as would be expected from the hitherto known literature values (Table 3). The substantial difference between the results obtained for $SeO(b0^+)$ with the two experimental methods and the large discrepancy of the literature data for $NCl(b^1\Sigma^+)$ point to the difficulties and error sources inherent in the experimental determination of such long lifetimes. These lifetimes can only be considered to be reliable when confirmed by different experimental techniques and different research groups. In view of our result for the heavier species PCl we suspect that both literature values for NCl(b) are too low. This assumption is supported by the theoretical result of Bettendorf [25]. The good agreement of the experimental lifetimes of the $b^1\Sigma^+$ state of SO and of the $a^1\Delta$ and $b^1\Sigma^+$ states of O_2 and NF with the recent theoretical results of Klotz *et al.* [23] and of Bettendorf [25] suggest that the theoretical data for the a states of SO and S_2 are at least of the right order of magnitude. The $a^1\Delta$ state lifetimes of SO and S_2 are certainly long enough to make these metastable molecules interesting energy carriers and reactants in chemical systems. For the antimony-containing species SbF, SbCl and SbBr which all show angular momentum coupling according to Hund's case c, the $b0^+$ state lifetime seems to increase with increasing size of the halogen atom. Coupled with this lifetime trend, a systematic change of the branching ratio of the intensities of the $b \rightarrow X_1$ and $b \rightarrow X_2$ subtransitions is observed [11, 12, 45].

4.4. Quenching processes

Many studies, both experimental and theoretical, have been made of the collisional quenching of the metastable $a^1\Delta_g$ and $b^1\Sigma_g^+$ states of O_2 [46]. It is generally assumed that quenching of the $O_2(b^1\Sigma_g^+)$ state proceeds by spin-allowed processes to the $a^1\Delta_g$ levels and that, for molecular quenchers, the dominant contribution to the quenching rates comes from state-to-state electronic-to-vibrational (E → V) energy transfer processes which convert the minimum amount of energy into product translation and rotation [32, 47 - 49]. This is strongly indicated by the finding that H_2 is about a factor of 60 more efficient in quenching $O_2(b^1\Sigma_g^+)$ than D_2. However, measurements of absolute efficiencies for some specific E → V processes made by Thomas and Thrush [50] contradicted the idea that energy resonances play an important role in the quenching processes of $O_2(b^1\Sigma_g^+)$. The observation of a common linear suprisal plot for the quenching of $O_2(b^1\Sigma_g^+)$ and $O_2(a^1\Delta_g)$ led these researchers to suggest a common non-specific quenching mechanism for both states with the processes occurring mostly on the repulsive part of the interaction potential.

Figure 12 shows the energy differences between the $b^1\Sigma^+$ and $a^1\Delta$ states of O_2, SO, SeO and S_2 and the low vibrational levels of some diatomic molecules. Since the Franck–Condon factors strongly favour $\Delta v = 0$ processes in the b → a transitions, near resonances between ΔE(b–a) and the vibrational levels of the quenchers are probably most important for the efficiencies of the E → V energy transfer processes. As is seen from Fig. 12, some much closer resonances occur for SO, SeO and S_2 than for O_2 which should show up in the quenching rate constants. The results in Table 4 show that the $b^1\Sigma^+$ quenching rate constants of SO and SeO in collisions with H_2 and D_2 are about a factor of 10 larger than for O_2. This is readily understood from the smaller energy defects of the E → V energy transfer processes and

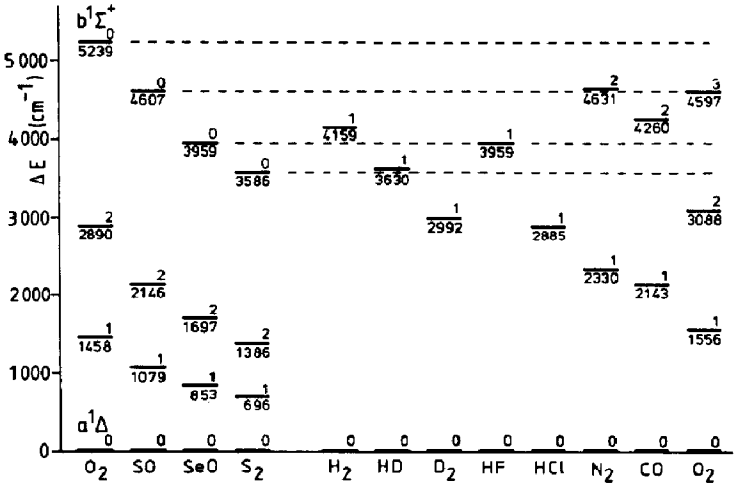

Fig. 12. Energy level diagram of the $a^1\Delta$ and $b^1\Sigma^+$ states of O_2, SO, SeO and S_2 and the vibrational states of diatomic molecules.

the larger b → a transition moments expected for these molecules. The ratio of the efficiencies of H_2 and D_2 which is 58 for O_2 increases to 92 for SO and is 43 for SeO. Both the larger value for SO and the lower value for SeO can be understood from the different energy resonances involved. Whereas for SO both processes are still exothermic but have smaller energy defects, for SeO(b) + H_2 the E → V transfer process is slightly endothermic which should reduce the H_2 rate constant and hence the ratio of the H_2 to D_2 efficiencies by about a factor of 3.

For PCl($b^1\Sigma^+$) the quenching rate constants of H_2 and D_2 are smaller and differ only by a factor of 3. As is seen from the data in Table 5 and Fig. 10, the energy defect for PCl(b) + H_2 is about 1300 cm^{-1} which is even larger than for O_2(b). This explains the rather low values of the rate constants and the smaller ratio. For S_2, E → V transfer from $S_2(b^1\Sigma_g^+, v = 0)$ to H_2 is endothermic by about 600 cm^{-1}. Preliminary Stern–Volmer measurements in the $O_2(a^1\Delta_g)$-sensitized chemiluminescence system indicate that in this case the ratio of the quenching efficiencies is inverted, *i.e.* D_2 quenches the S_2(b) state more strongly than H_2 does. In our previous spectroscopic studies very strong H_2–D_2 "isotope effects" were also found for the quenching of the $b0^+$ states of TeO, TeS, TeSe and Te_2 [7, 8]. As is seen from Fig. 9, the energy separations of the $b0^+$ and a2 states in these molecules are probably all near 4159 cm^{-1}, the vibrational energy $H_2(v = 1)$, such that very efficient quenching by H_2 is to be expected. In all cases the H_2 and D_2 quenching rate constants thus indicate the importance of energy resonances and E → V transfer processes.

As is seen from Fig. 12, a close energy resonance occurs in the quenching of SO($b^1\Sigma^+$) by N_2. The data in Table 4 show that for O_2, SeO and PCl nitrogen is a rather inefficient quencher of the $b^1\Sigma^+$ states, and that CO in all cases is more efficient than N_2. For SO($b^1\Sigma^+$) the opposite is true; N_2 is more efficient than CO and its rate constant is larger by at least a factor of 40 compared with O_2, SeO and PCl. These results strongly indicate that the $\Delta v = 2$ E → V energy transfer

$$SO^{**}(b, v = 0) + N_2(v = 0) \longrightarrow SO^{*}(a, v = 0) + N_2(v = 2) - 24\ cm^{-1} \qquad (13)$$

is indeed the dominant process. Evidently, more detailed studies including measurements of the temperature dependences of the quenching rate constants for the near-resonant processes are necessary to obtain a more quantitative understanding of the mechanism involved.

4.5. Population inversions between vibronic states

The efficient near-resonant energy exchange processes between $O_2(a^1\Delta_g)$ and S_2, SeS, Se_2 and TeS lead to the question whether population inversion occurs between vibronic levels of these molecules in the $O_2(a^1\Delta_g)$-sensitized systems. When the collisional equilibrium (1) and the quenching processes

$$S_2^{**}(b) + M \xrightarrow{k_{S_2^{**}}^{q}} S_2^{*}(a) + M \qquad (14)$$

$$S_2^*(a) + M \xrightarrow{k_{S_2^*}{}^q} S_2(X) + M \tag{15}$$

are considered and it is assumed that all radiative processes are negligible compared with collision-induced processes, the steady state rate equation for $S_2^*(a)$ is

$$\frac{d[S_2^*]}{dt} = 0$$

$$= k_{S_2^{**}}{}^q[S_2^{**}][M] - k_{S_2^*}{}^q[S_2^*][M] \tag{16}$$

Substituting $[S_2^{**}]$ from eqn. (4) and rearranging

$$\frac{[S_2^*]}{[S_2]} = K \frac{k_{S_2^{**}}{}^q}{k_{S_2^*}{}^q} \frac{[O_2^*]}{[O_2]} \tag{17}$$

is obtained. With $K \approx 0.6$ and $[O_2^*]/[O_2] \approx 0.01$ population inversion would occur if the ratio of the quenching rate constants is about 200 or more. For O_2, "normal quenchers" have $O_2(b\,^1\Sigma_g^+)$ quenching rate constants which are four to five orders of magnitude larger than the corresponding values for $O_2(a\,^1\Delta_g)$ [46]. Therefore, it may be expected that for S_2 the ratio of the quenching rate constants is also large enough to give strong population inversion between the $a\,^1\Delta_g$ and $X\,^3\Sigma_g^-$ states. The same will probably be true for SeS, Se_2 and TeS. Similar estimations show that population inversion may also occur between the $b\,^1\Sigma^+, v' = 0$ and the higher vibrational levels $v'' = 1$ and $v'' = 2$ of the $X_1 0^+$ and $X_2 1$ ground states of these molecules. A better knowledge of the radiative lifetimes, energy exchange and quenching processes is necessary to estimate whether a measurable gain or laser action can be achieved in some of the transitions.

Acknowledgments

Financial support of this work by the Deutsche Forschungsgemeinschaft (projects SFB 42/B2 and Fi 141/9-1), the Ministerium für Wissenschaft und Forschung des Landes Nordrhein–Westfalen and the Fonds der Chemischen Industrie is gratefully acknowledged.

References

1 K. P. Huber and G. Herzberg, *Molecular Spectra and Molecular Structure*, Vol. 4, *Constants of Diatomic Molecules*, Van Nostrand, Princeton, NJ, 1979.
2 I. Barnes, K. H. Becker and E. H. Fink, *Chem. Phys. Lett.*, *67* (1979) 310.
3 S. P. Reddy and K. K. Verma, *J. Mol. Spectrosc.*, *84* (1980) 89.
4 A. T. Pritt, Jr., D. Patel and R. D. Coombe, *J. Mol. Spectrosc.*, *87* (1981) 401.

5 I. Barnes, K. H. Becker and E. H. Fink, *Chem. Phys. Lett.*, *67* (1979) 314.
6 R. Winter, I. Barnes, E. H. Fink, J. Wildt and F. Zabel, *Chem. Phys. Lett.*, *73* (1980) 297.
7 R. Winter, I. Barnes, E. H. Fink, J. Wildt and F. Zabel, *Chem. Phys. Lett.*, *86* (1982) 118.
8 R. Winter, I. Barnes, E. H. Fink, J. Wildt and F. Zabel, *J. Mol. Struct.*, *80* (1982) 75.
9 R. Winter, E. H. Fink, J. Wildt and F. Zabel, *Chem. Phys. Lett.*, *94* (1983) 335.
10 H. Kruse, R. Winter, E. H. Fink, J. Wildt and F. Zabel, to be published.
11 R. Winter, H. Kruse, E. H. Fink, J. Wildt and F. Zabel, *Chem. Phys. Lett.*, *104* (1984) 383.
12 H. Kruse, R. Winter, E. H. Fink, J. Wildt and F. Zabel, *Chem. Phys. Lett.*, *93* (1982) 475.
13 R. Winter, H. Kruse, E. H. Fink and J. Wildt, *Chem. Phys. Lett.*, *102* (1983) 404.
14 J. Wildt, G. Elfers, M. Bielefeld and E. H. Fink, to be published.
15 J. Wildt, E. H. Fink, R. Winter and F. Zabel, *Chem. Phys.*, *80* (1983) 167.
16 I. Kovacs, *Rotational Structure in the Spectra of Diatomic Molecules*, Hilger, London, 1969.
17 J. K. G. Watson, *Can. J. Phys.*, *46* (1968) 1637.
18 G. Herzberg, *Molecular Spectra and Molecular Structure*, Vol. 1, *Spectra of Diatomic Molecules*, Van Nostrand, Princeton, NJ, 1965.
19 T. Amano, E. Hirota and Y. Morino, *J. Phys. Soc. Jpn.*, *22* (1967) 399.
20 R. Colin, *Can. J. Phys.*, *46* (1968) 1538.
21 W. J. Clark and F. C. De Lucia, *J. Mol. Spectrosc.*, *60* (1976) 332.
22 C. Long and D. R. Kearns, *J. Chem. Phys.*, *59* (1973) 5729.
23 R. Klotz, C. M. Marian, S. D. Peyerimhoff and R. J. Buenker, submitted to *Chem. Phys.*
24 R. J. Malins and D. W. Setser, *J. Phys. Chem.*, *85* (1981) 1342.
25 M. Bettendorf, *Dissertation*, Universität Bonn, Bonn, 1984.
26 P. H. Tennyson, A. Fontijn and M. A. A. Clyne, *Chem. Phys.*, *62* (1981) 171.
27 R. D. Coombe, D. Patel, A. T. Pritt, Jr., and F. W. Wodarczyk, *J. Chem. Phys.*, *75* (1981) 2177.
28 F. R. Burden, M. A. A. Clyne and A. Fontijn, *Chem. Phys.*, *65* (1982) 123.
29 K. H. Becker, W. Groth and U. Schurath, *Chem. Phys. Lett.*, *8* (1971) 259.
30 K. Kohse-Höinghaus and F. Stuhl, *J. Chem. Phys.*, *72* (1980) 3720.
31 L. R. Martin, R. B. Cohen and J. F. Schatz, *Chem. Phys. Lett.*, *41* (1976) 394.
32 K. Kear and E. W. Abrahamson, *J. Photochem.*, *3* (1975) 409.
33 J. A. Davidson, K. E. Kear and E. W. Abrahamson, *J. Photochem.*, *1* (1973) 307.
34 F. Ahmed and R. F. Barrow, *J. Phys. B*, *7* (1974) 2256.
35 H. Kruse, R. Winter and E. H. Fink, to be published.
36 V. E. Bondybey and J. H. English, *J. Chem. Phys.*, *72* (1980) 3113.
37 C. Effantin, J. d'Incan, J. Vergès, M. T. McPherson and R. F. Barrow, *Chem. Phys. Lett.*, *70* (1980) 560.
38 U. Schurath, personal communication, 1984.
39 T. Ishiwata and I. Tanaka, *13th Int. Conf. on Photochemistry, Clearwater Beach, FL, 1978*.
40 W. H. Breckenridge and T. A. Miller, *J. Chem. Phys.*, *56* (1972) 465.
41 S. J. Arnold, N. Findlayson and E. A. Ogryzlo, *J. Chem. Phys.*, *44* (1966) 2529.
42 W. Hack and O. Horie, *Chem. Phys. Lett.*, *82* (1981) 327.
43 M. A. Kwok and J. M. Herbelin, in L. E. Wilson, S. N. Suchard and J. I. Steinfeld (eds.), *Electronic Transition Lasers*, Vol. II, Massachusetts Institute of Technology Press, Cambridge, MA, 1977, p. 100.
44 R. G. Derwent and B. A. Thrush, *Discuss. Faraday Soc.*, *53* (1972) 162.
45 R. Colin, M. Herman and F. Prevot, *Chem. Phys. Lett.*, *91* (1982) 213.
46 E. A. Ogryzlo, in H. H. Wasserman and R. W. Murray (eds.), *Singlet Oxygen*, Academic Press, New York, 1979, p. 35.

47 J. A. Davidson and E. A. Ogryzlo, in M. J. Cormier, D. M. Hercules and J. Lee (eds.), *Chemiluminescence and Bioluminescence*, Plenum, New York, 1973, p. 111.
48 M. Braithwaite, J. A. Davidson and E. A. Ogryzlo, *J. Chem. Phys.*, *65* (1976) 771.
49 M. Braithwaite, E. A. Ogryzlo, J. A. Davidson and H. I. Schiff, *Chem. Phys. Lett.*, *42* (1976) 158.
50 R. G. O. Thomas and B. A. Thrush, *Proc. R. Soc. London, Ser. A*, *356* (1977) 287, 295, 307.